Synthesis, Structural Studies, and Magnetic Properties of a New Mixed-Valence Diphosphate: $Zn^{2+}{}_5Fe^{3+}{}_2(P_2O_7)_4$

H. Lamsaf, E. H. Elghadraoui, R. Fausto, A. Oulmekki & B. F. O. Costa

Journal of Superconductivity and Novel Magnetism

ISSN 1557-1939

J Supercond Nov Magn
DOI 10.1007/s10948-019-05263-w

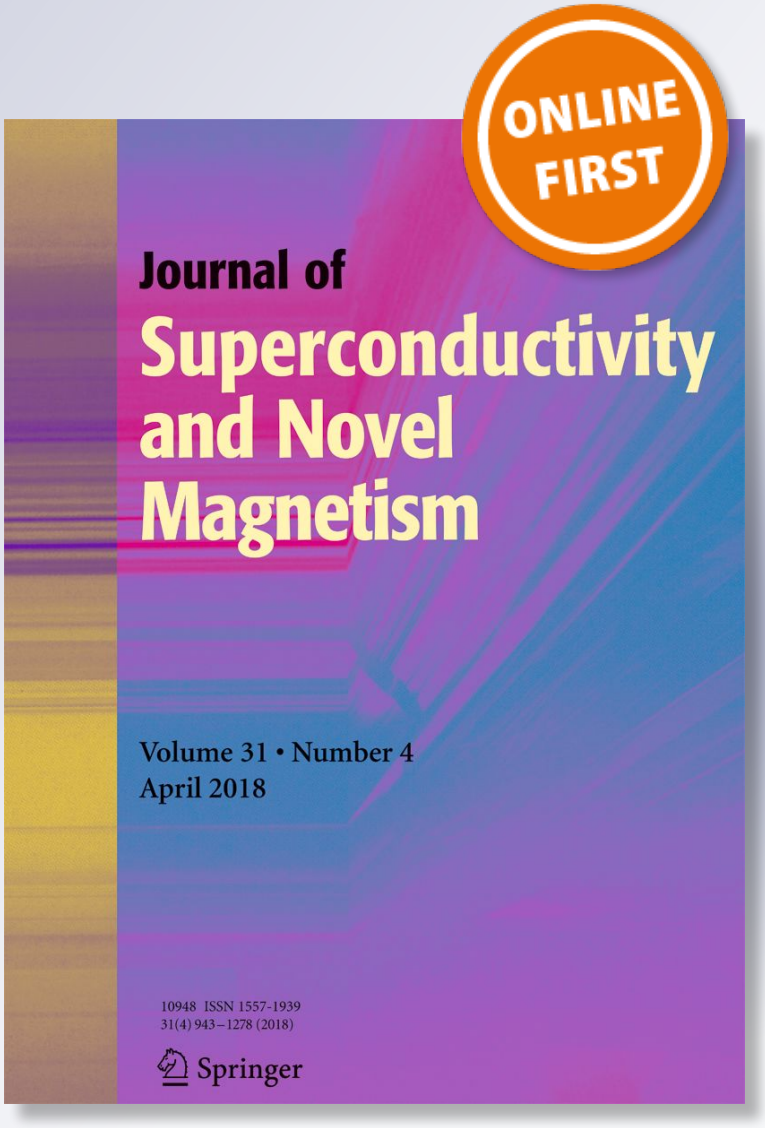

Springer

Journal of Superconductivity and Novel Magnetism
https://doi.org/10.1007/s10948-019-05263-w

ORIGINAL PAPER

Synthesis, Structural Studies, and Magnetic Properties of a New Mixed-Valence Diphosphate: $Zn^{2+}{}_5Fe^{3+}{}_2(P_2O_7)_4$

H. Lamsaf[1] · E. H. Elghadraoui[1] · R. Fausto[2] · A. Oulmekki[1] · B. F. O. Costa[3]

Received: 19 February 2019 / Accepted: 14 August 2019

Abstract
A new mixed-valence diphosphate, $Zn^{2+}{}_5Fe^{3+}{}_2(P_2O_7)_4$, was synthesized from $Fe^{II}{}_5Fe^{III}{}_2(P_2O_7)_4$ via the "solid way" route, by substitution of Fe^{II} by Zn^{II}. The obtained X-ray data confirmed the crystallization of the compound in the $C222_1$ symmetry space group (orthorhombic). Magnetic measurements were performed showing that, at room temperature, the compound is paramagnetic and that the Néel temperature is 15.44(20) K. The compound was also investigated by infrared and Raman spectroscopies, in particular to characterize the $(P_2O_7)^{4-}$ and M–O vibrations.

Keywords New mixed-valence diphosphate · X-ray diffraction · Raman and infrared spectroscopies · Magnetometry

1 Introduction

Phosphates exhibit many useful properties for industrial applications, and they have been considered good candidates for encapsulation of nuclear wastes [1]. They have also demonstrated importance in catalysis [2, 3]. However, according to the World Health Organization [4], the current processes in the phosphate industry generate significant amounts of solid waste containing dangerous substances, such as metallic trace elements (TMEs) that, beyond the authorized concentrations, are known to be very harmful for the environment and the health [5]. The need for novel phosphate-based materials and new production techniques that might reduce the environmental and health impact is then well recognized worldwide, and justifies the great attention given to these subjects in the last few decades. Morocco is one of the major producers of phosphates at world scale, and the present work is in line with the national strategic plan for valorization of phosphates by means of chemical recycling using phosphate-based matrices as useful carriers for metallic trace elements [6].

Different types of phosphates have dissimilar magnetic properties ($AgFeP_2O_7$ [7], $Na_{2-x}(Fe_{1-y}Mn_y)P_2O_7$ [8], $Na_2Pb_{1-x}Cu_xP_2O_7$ [9]), so that the study of phosphates magnetism is desirable. In this study, we have focused on a Zn^{2+} compound belonging to the pyrophosphate (diphosphate) family of compounds $[Zn^{II}{}_5Fe^{III}{}_2(P_2O_7)_4]$, for which the mixed-valence iron derivative $Fe^{II}{}_5Fe^{III}{}_2(P_2O_7)_4$ (or, in a simplified way, $Fe_7(P_2O_7)_4$) can be considered the parent species [10].

Derivatives of iron pyrophosphate, where the Fe^{II} ion has been replaced by Cd^{II} and the Fe^{III} by V^{III}, have been investigated previously [11, 12]. The $Cd_5M_2(P_2O_7)_4$ (M = Fe, V) [11] and $Cd_{4.12}Fe_{0.83}Fe_2(P_2O_7)_4$ [12] diphosphates were found to be isostructural with $Fe_7(P_2O_7)_4$. On the other hand, recent investigations reporting the successful substitution of the Fe^{II} ion by Zn^{II} in the mix-valence $Fe_3(P_2O_7)_2$ compound $[Fe^{II}Fe^{III}{}_2(P_2O_7)_2]$ concluded that the zinc substituted derivative exhibits interesting magnetic properties with an antiferromagnetic behavior at a Neel temperature of 5 K and 15 K for $Zn^{II}Fe^{III}{}_2(P_2O_7)_2$ and $Zn_{0.5}{}^{II}Cu_{0.5}{}^{II}Fe^{III}{}_2(P_2O_7)_2$, respectively [13–15]. The magnetic results on $Fe_7(P_2O_7)_4$ ($Fe_5{}^{2+}Fe_2{}^{3+}(P_2O_7)_4$) showed an antiferromagnetic behavior with a Neel temperature of 25 K. In the paramagnetic domain, above 40 K, the Curie-Weiss law is obeyed [16]. These later results encouraged us to prepare the zinc derivative of iron pyrophosphate where the Fe^{II} ion is replaced by Zn^{II},

✉ B. F. O. Costa
benilde@uc.pt

[1] Chemistry Laboratory of Condensed Matter (LCMC), Faculty of Science and Technology Fez, University of Sidi Mohammed Ben Abdellah, BP. 2202, Fes, Morocco

[2] CQC, Department of Chemistry, University of Coimbra, P-3004-535 Coimbra, Portugal

[3] CFisUC, Department of Physics, University of Coimbra, P-3004-516 Coimbra, Portugal

Published online: 13 September 2019

$Zn^{II}{}_5Fe^{III}{}_2(P_2O_7)_4$, and characterize it structurally and magnetically.

Below, the synthetic procedure used to produce the new diphosphate is first described, followed by the characterization of the compound by X-ray diffraction and energy-dispersive X-ray analysis, complemented by infrared and Raman spectroscopic studies. Finally, magnetometry was used to investigate the magnetic properties of the synthesized new phosphate.

2 Experimental

2.1 Synthesis

The procedure used to synthesize the $Zn_5Fe_2(P_2O_7)_4$ pyrophosphate follows that described in refs. [13, 14] and has been designated as "dry way" method. Briefly, stoichiometric amounts of ZnO, Fe_2O_3, and $(NH_4)HPO_4$ were used as starting materials. After milling for 1 h, the solid solution was heat-treated at temperatures up to 850 °C for 24 h, affording the desired material. The heat treatment was interrupted periodically for grinding, to ensure homogeneity.

2.2 Methods and Instrumentation

X-ray diffraction (XRD) was used to structurally characterize the sample powder at room temperature. A Cu-kα anode (1.541874 Å) was used, with a step size of 0.02°. The refinement of the lattice parameters was carried out by the Rietveld method using the HighScore Plus software [17], and the graphical representation of the crystalline structure was done using the VESTA software [18], based on the structure CIF file predicted by the program www.Materialsproject.com. This last program used generates the structures by substitution on known compounds using data-mining strategies from the ICSD database [19]. Crystallite size (Dsc) was calculated from the full-width-at-half-height (FWHM) of the diffraction pattern peaks, using the Scherrer equation [20].

Energy-dispersive X-ray analysis (EDXA) was performed with a QUANTA 200FEI microscope, operating at a voltage of 20 kV, and equipped with a Burker XFlagh 410M EDXA detector. These experiments allowed the identification of the sample's elemental composition. For the analysis, a small pellet of the compound under investigation was placed on a carbon tape.

The infrared spectroscopy experiments were done in the mid-IR range, at room temperature, using the KBr pellet technique, in a JASCOFTIR 4200 spectrometer, with 4 cm^{-1} resolution and 64 scans.

The Raman spectroscopy data were collected in the 400 to 1200 cm^{-1} Raman shift range with a Raman SENTERRA system (Bruker), using as excitation source a diode laser operating at 785 nm, and a laser power of 10 mW. The integration time selected was 20 s and the number of scans added was 16.

Magnetometry measurements were done in a vibrating sample magnetometer (VSM) fitted with a cryogen-free Physical Properties Measurement System (DynaCool PPMS), and operating at a vibration frequency of 40 Hz and an amplitude of 2 mm in the central area of the coils, where the powder sample was placed in a rod-shaped Perspex sample holder.

3 Results and Discussions

3.1 X-ray Diffraction and Energy-Dispersive X-ray Analysis Studies

Figure 1 shows the X-ray diffraction pattern of the studied diphosphate, $Zn_5Fe_2(P_2O_7)_4$, obtained at room temperature. It was indexed to an orthorhombic structure belonging to the $C222_1$ space group. The data show good correspondence to the X-ray diffraction pattern of iron diphosphate, $Fe^{II}{}_5Fe^{III}{}_2(P_2O_7)_4$ [10], thus following the same trend previously observed for $Cd_5M_2(P_2O_7)_4$ (M = Fe, V) diphosphates [11], which were also found to be isostructural to $Fe_7(P_2O_7)_4$ [10]. The same was found for $Cd_{4.12}Fe_{0.83}Fe_2(P_2O_7)_4$ [12].

The refined unit cell crystals for parameters of $Zn_5Fe_2(P_2O_7)_4$ are shown in Table 1, where they are compared with those reported before for $M^{II}{}_5M'^{III}{}_2(P_2O_7)_4$ (M = Zn, Fe, Cd; M' = Fe, V) [10–12, 21]. The unit cell parameters show increasing values according to the order $Zn^{2+} < Fe^{2+} < Cd^{2+}$, and also with the substitution of $Fe^{3+}$by V^{3+}. These trends are in good agreement with the relative sizes of the ions: $R(Zn^{2+}) = 0.74$ Å; $R(Fe^{2+}) = 0.77$ Å; $R(Cd^{2+}) = 0.95$ Å; and $R(Fe^{3+}) = 0.55$ Å; $R(V^{3+}) = 0.64$ Å [22, 23], where R stays for the ionic radii.

The $Zn_5Fe_2(P_2O_7)_4$ diphosphate develops in an orthorhombic $C222_1$ symmetry space group crystal, which is formed by a series of polyhedra: ZnO_6 and FeO_6 octahedra, and PO_4 tetrahedra belonging to two different phosphate groups.

Figure 2 shows a representation of the crystalline structure of $Zn_5Fe_2(P_2O_7)_4$, which was obtained as described in Section 2.2. The crystalline structure consists of layers composed of rows of FeO_6 and ZnO_6 octahedra (shown in red and blue colors, respectively, in Fig. 2). The three-dimensional arrangement of these layers is provided through the diphosphate groups (in yellow).

The obtained average value of the crystallite size (Dsc = 24.30 nm) confirms that the prepared $Zn_5Fe_2(P_2O_7)_4$

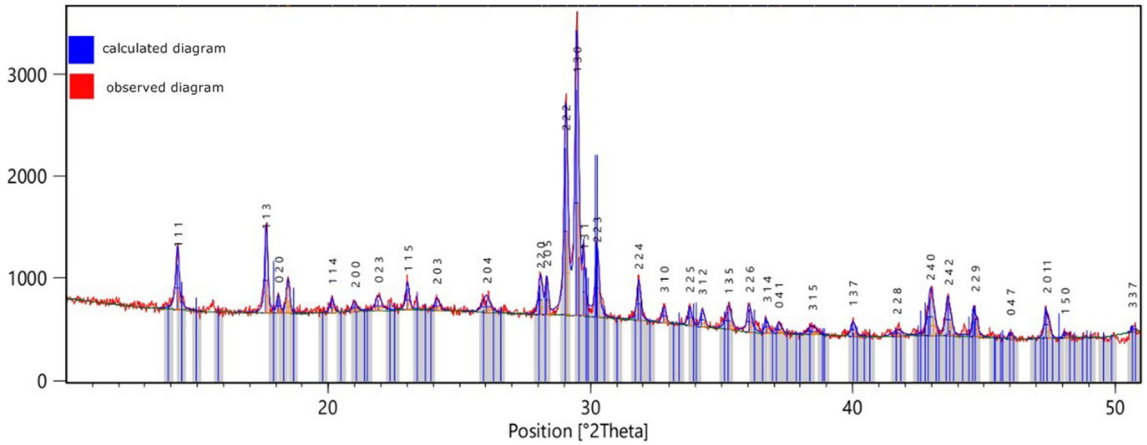

Fig. 1 Observed, calculated diagrams of X-ray diffraction and hkl data refinement $Zn_5Fe_2(P_2O_7)_4$ powder

diphosphate material possesses nanometric dimension. According to the literature [24], this grains' size is appropriate to facilitate the chemisorption of oxygen.

The EDXA experiments were used to confirm the elemental composition of the studied compound. As expected, all peaks of Zn, Fe, P, and O are present in the EDXA spectrum presented in Fig. 3. This shows that all the elements are not volatile at the maximum temperature during the synthesis (850 °C). The carbon peak around 0 keV is due to the carbon present in the support material of the sample used in the analysis (see Section 2.2).

3.2 Infrared and Raman Spectroscopic Studies

Figures 4 and 5 present the room temperature infrared and Raman spectra of $Zn_5Fe_2(P_2O_7)_4$, respectively. The comparison of these spectra with those previously reported for other diphosphates [13, 14, 24–29] allowed characterization of the vibrations associated with the diphosphate fragment, as well as those associated with the Zn-O and Fe-O moieties.

In the infrared spectrum of the compound (Fig. 4), no bands are observed between 1800 and 1400 cm^{-1}, allowing to conclude on the absence of water molecules in the sample and, thus, confirming that the synthesized material is anhydrous. In the 1300–600 cm^{-1} region, the infrared spectrum shows a considerably large number of broad bands of variable intensity. The stretching modes of the terminal PO_3^{2-} groups give rise to two broad intense pairs of bands, at 1273/1081 cm^{-1} and 1011/938 cm^{-1}, which are ascribed to the anti-symmetric and symmetric stretching modes of these groups, respectively. In turn, the symmetric P-O stretching mode of the bridges is observed at 850 cm^{-1}, while the bands at 576, 551, and 521 cm^{-1} are attributed to deformation modes of the PO_3^{2-} groups [13, 14].

In the Raman spectrum (Fig. 5), the bands due to the stretching modes of the PO_3^{2-}groups are observed at 1200 cm^{-1} (anti-symmetric modes) and 1000 cm^{-1} (symmetric), in good agreement with the data reported in refs. [27–29] for $Fe_4(P_2O_7)_2$, $Zn_2Fe(PO_4)_2{\cdot}4H_2O$, $ZnFe_2(P_2O_7)_2$, and $Zn_{0.5}Cu_{0.5}Fe_2(P_2O_7)_2$, while the bands observed at 960 and 910 cm^{-1} are attributed, respectively, to the anti-symmetric and symmetric stretching vibrations of the POP bridge [27–29]. The deformation vibrations of the diphosphate moiety and the Zn-O and Fe-O stretching modes give rise to bands at frequencies within the 600–450 cm^{-1} range, also in good agreement with previously reported data [13, 14, 26–29].

Table 1 Crystal unit cell parameters (unit cell axes, *a*, *b*, *c*, and volume, V) for $M^{II}_5M'^{III}_2(P_2O_7)_4$ (M = Zn, Fe, Cd; M' = Fe, V)

	a/Å	*b*/Å	*c*/Å	V/Å^3
$Zn_5Fe_2(P_2O_7)_4$	8.415(6)	9.696(6)	23.666 (9)	1931.2(9)
$Fe_5Fe_2(P_2O_7)_4$	8.451(1)[a]; 8.4327(7)[b]	9.691(1)[a]; 9.695(1)[b]	23.626(5)[a]; 23.663(4)[b]	1934.9(9)[a]; 1934.0(0)[b]
$Cd_{4.12}Fe_{0.83}Fe_2(P_2O_7)_4$	8.702(1)	9.889(1)	23.968(3)	2062.5(3)
$Cd_5Fe_2(P_2O_7)_4$	8.715(6)	9.9217(7)	23.999(1)	2086.0(2)
$Cd_5V_2(P_2O_7)_4$	8.778(7)	9.9282(8)	24.037(2)	2094.5(6)

[a] From ref. [10]

[b] From ref. [21]

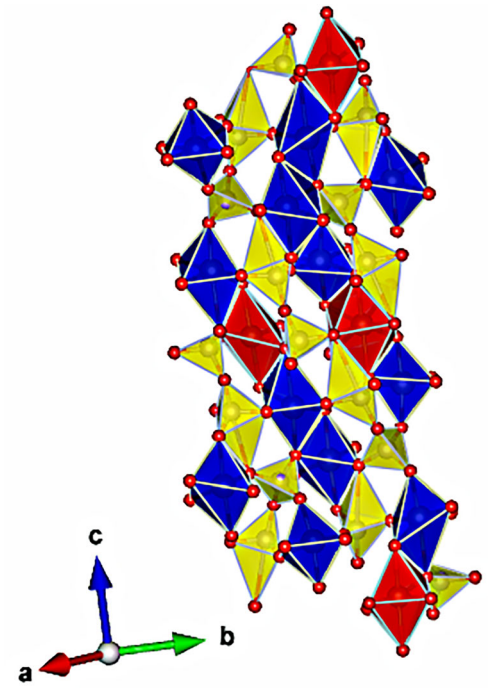

Fig. 2 Crystalline structure of $Zn_5Fe_2(P_2O_7)_4$. FeO_6, ZnO_6, and diphosphate moieties are represented in red, blue, and yellow, respectively. Oxygen atoms are shown as light red circles

3.3 Magnetic Measurements

Figures 6 and 7 show the field cooled (FC) and zero field cooled (ZFC) curves in an applied field of 500 Oe, and the inverse of magnetic susceptibility ($1/\chi$), respectively. At the Néel temperature, $T_N = 15.44(20)$ K, an antiferromagnetic-paramagnetic transition occurs. The Curie-Weiss law is obeyed above T_N, with a Curie temperature $\theta_p = -56.6(1)$ K and a Curie constant $C = 12.1(1)$ emu g^{-1} K^{-1}. This last value corresponds to an apparent effective magnetic moment of $\mu_{eff} = 9.87$ μ_B.

The negative value of the Curie temperature indicates the presence of antiferromagnetic interactions, as already seen in the $Fe_7(P_2O_7)_4$ diphosphate [10, 16]. In this last case, the obtained values for the Néel and Curie temperatures were $T_N = 25$ K and $\theta_p = -25$ K [10].

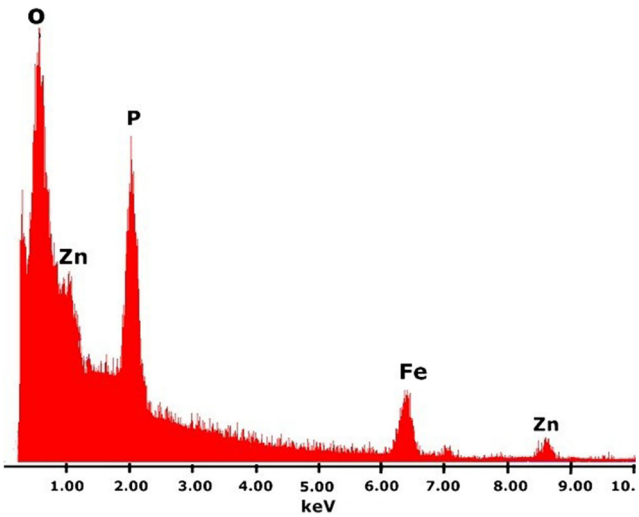

Fig. 3 EDXA spectrum of $Zn_5Fe_2(P_2O_7)_4$

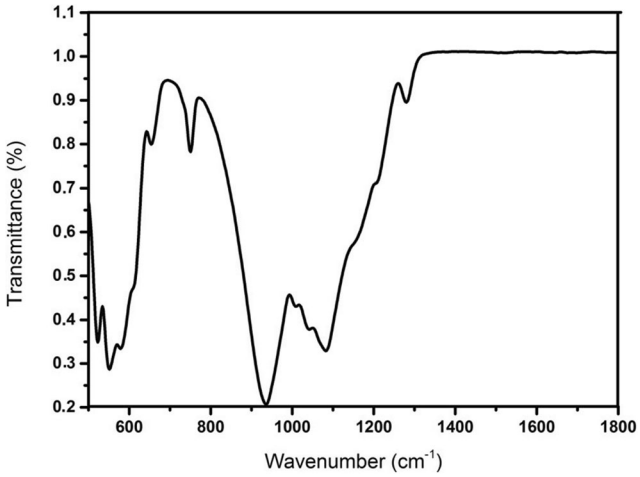

Fig. 4 Room temperature infrared spectrum of $Zn_5Fe_2(P_2O_7)_4$ in KBr pellet

4 Conclusion

The substitution of Fe^{II} in $Fe^{II}{}_5Fe^{III}{}_2(P_2O_7)_4$ diphosphate by Zn^{II} gave a new diphosphate, $Zn^{II}{}_5Fe^{III}{}_2(P_2O_7)_4$, which was structurally characterized and investigated in relation with its spectroscopic and magnetic properties. The refined X-ray diffraction pattern shows that the new phosphate crystallizes in the orthorhombic $C222_1$ symmetry space group, being

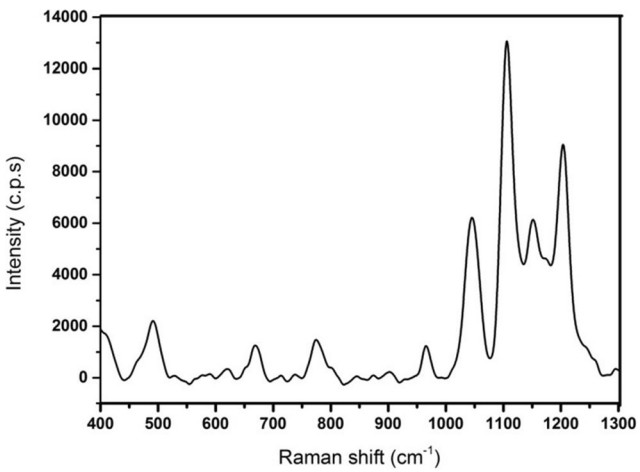

Fig. 5 Room temperature Raman spectra of $Zn_5Fe_2(P_2O_7)_4$ (powder)

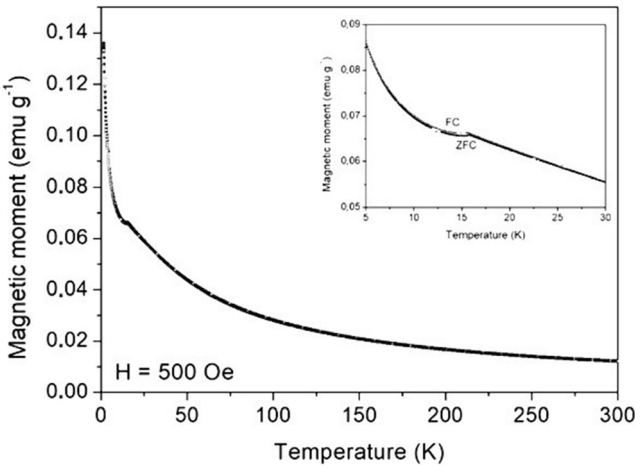

Fig. 6 FC and ZFC curves of $Zn_5Fe_2(P_2O_7)_4$ diphosphate measured in a field of 500 Oe

isostructural with $Fe_7(P_2O_7)_4$. Details of the crystalline structure of the zinc diphosphate were discussed and compared with other diphosphates. The infrared and Raman spectra allowed characterizing vibrationally the material, in particular in what concerns to the phosphates and M-O vibrations. An antiferromagnetic-paramagnetic transition was shown to occur at $T_N = 15.44(20)$ K.

An antiferromagnetic-paramagnetic transition has been found before for $Fe^{II}_5Fe^{III}_2(P_2O_7)_4$ diphosphate [10, 16]. Then, the present study reveals that the substitution of Fe^{II} by Zn^{II} in this type of materials leads to isostructural diphosphates to the mixed-valence iron diphosphate, and also that the $Zn^{II}Fe^{III}$ materials also exhibit predominant antiferromagnetic interactions, with a smaller T_N. These results stress the relevance of further studying mixed zinc-iron phosphates, which appear as appropriate materials for magnetic applications.

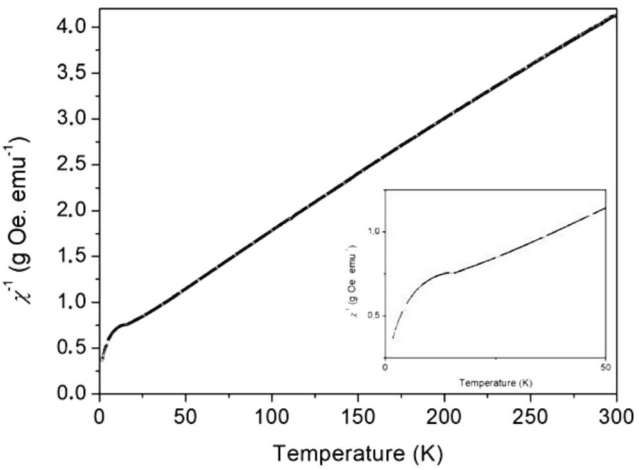

Fig. 7 Temperature dependence of the inverse of the magnetic susceptibility of $Zn_5Fe_2(P_2O_7)_4$

Funding Information This work was partially supported by funds from FEDER (Programa Operacional Factores de Competitividade COMPETE) and from FCT-Fundação para a Ciência e a Tecnologia under the Project No. UID/FIS/04564/2016. Access to TAIL-UC (VSM measurements) was funded under QREN-Mais Centro Project ICT-2009-02-012-1890. The Coimbra Chemistry Center (CQC) is also supported by FCT (Project UI0313/QUI/2013) and COMPETE. R.F. also acknowledges the Portugal 2020 Project MATIS.

References

1. Mayr, W.: Biochem. J. **2**, 585–591 (1988)
2. Bonnet, P., Millet, J.M.M., Leclercq, C., Védrine, J.C.: J. Catal. **158**, 128–141 (1996)
3. Bonnet, P., Millet, J.M.M.: J. Catal. **161**, 198–205 (1996)
4. Health Risks of Heavy Metals from Long-range Transboundary Air Pollution, Annual Report of the World Health Organization (2007)
5. Biney, C., Amuzu, A.T., Calamari, D., Kaba, N., Mbome, I.L., Naeve, H., Ochumba, O., Osibanjo, O., Radegonde, V., Saad, M.A.H.: FAO Fish. Rep. (1992)
6. 1ères Assises Nationales de R&D Autour des Phosphates: Skhirat. (2013)
7. Terebilenko, K.V., Kirichok, A.A., Baumer, V.N., Sereduk, M., Slobodyanik, N.S., Gütlich, P.: J. Solid State Chem. **183**(6), 1473–1476 (2010)
8. Barpanda, P., Liu, G., Mohamed, Z., Ling, C.D., Yamada, A.: Solid State Ionics. **268**, 305–311 (2014)
9. Abadi, S., Aride, J., Benkhouja, K., Haddad, M., Taibi, M.: Arab. J. Chem. (2017)
10. Malaman, B., Ijjaali, M., Gerardin, R., Venturini, G., Gleitzer, C.: Eur. J. Solid State Inorg. Chem. **29**, 1269–1284 (1992)
11. Boudin, S., Grandin, A., Labbe, P.H., Grebille, D., Nguyen, N., Ducourelle, A., Raveau, B.: J. Solid State Chem. **121**, 291–300 (1996)
12. Elbelghitti, A., Boukhari, A.: Acta Crystallogr. Sect. C. **50**, 1648–1650 (1994)
13. Lamsaf, H., Fausto, R., Costa, B.F.O., Toyir, J., Elghadraoui, E.H., Ijjaali, M., Oulmekki, A.: Mater. Chem. Phys. **216**, 22–27 (2018)
14. Lamsaf, H., Oulmekki, A., Elghadraoui, E.H., Fausto, R., Costa, B.F.O.: J. Phys. Chem. Solids. **119**, 122–125 (2018)
15. Lamsaf, H., Oulmekki, A., Elghadraoui, E.H., Fausto, R., Wagner, F.E., Costa, B.F.O.: J. Supercond. Nov. Magn. **32**, 1377 (2018). https://doi.org/10.1007/s10948-018-4848-8
16. Ijjaadi M., PhD Thesis, University of Fes, Morocco, 1994
17. X'PertHighScore Plus: PANalytical. Almelo B.V, Netherlands (2006)
18. Momma, K., Izumi, F.: VESTA 3. J.Appl. Crystallogr. **44**, 1272–1276 (2011)
19. Jain, A., Hautier, G., Moore, C., Ong, S.P., Fischer, C.C., Mueller, T., Persson, K.A., Ceder, G.: Comput. Mater. Sci. **50**, 2295–2310 (2011)
20. Guinier A., Dunod X. (Ed.), Theorie et Technique de la Radiocristallographie, third ed., 1964, p. 462
21. Genkina, E.A., Maksimov, B.A., Zvereva, O.V., Mininze, Yu, M., Lyubutin, I.S., Luchko, S.V., Yakovlev, V.V.: Sov. Phys. Crystallogr. **37**, 627–632 (1992)
22. Shannon, R.D.: Acta Crystallogr. A. **32**, 751–767 (1976)
23. Cullity, B.D., Stuart, R.S.: Elements of X-ray diffraction. Prentice Hall, Upper Saddle River, NJ (2001)
24. Ruette, F., Sierralta, A., Sánchez, M., Luiggi, N.: J. Comput. Meth. Sci. Eng. **17**, 55–62 (2017)
25. Baran, E.J., Mercader, R.C., Massaferro, A., Kremer, E.: Spectrochim. Acta A. **60**, 1001–1005 (2004)

26. Rulmont, A., Cahay, R., Liegeois-Duyckaerts, M., Tarte, P.: Eur. J. Solid State Inorg.Chem. **28**, 207–219 (1981)
27. Farmer, V.C.: The Infrared Spectra of Minerals, Minerals Soc. Publ., London (1974)
28. Zhang, L., Brow, R.K., Schlesinger, M.E., Ghussn, L., Zanotto, E.D.: J. Non-Cryst. Sol. **356**, 1252–1257 (2010)
29. Scholza, R., Frost, R.L., Xi, Y., Graça, L.M., Lagoeiro, L., López, A.: J. Mol. Struct. **1039**, 22–27 (2013)